Adsorption of tannic acid from aqueous solution onto surfactant-modified zeolite

Jianwei Lin [a,*], Yanhui Zhan [b], Zhiliang Zhu [b], Yunqing Xing [a]

[a] College of Marine Science, Shanghai Ocean University, No. 999 Hucheng Huan Road, Pudong District, Shanghai 201306, China
[b] State Key Laboratory of Pollution Control and Resource Reuse, Tongji University, Shanghai 200092, China

ARTICLE INFO

ABSTRACT

Surfactant-modified zeolites (SMZs) with various loadings of cetylpyridinium bromide (CPB) were used as adsorbents to remove tannic acid (TA) from aqueous solution. The TA adsorption efficiencies for natural zeolite and various SMZs were compared. SMZ presented higher TA adsorption efficiency than natural zeolite, and SMZ with higher loading amount of CPB exhibited higher TA adsorption efficiency. The adsorption of TA onto SMZ as a function of contact time, initial adsorbate concentration, temperature, ionic strength, coexisting Cu(II) and solution pH was investigated. The adsorbents before and after adsorption were characterized by X-ray diffraction (XRD), field emission scanning electron microscope (FE-SEM), thermogravimetric analysis (TGA), and Fourier transform infrared (FT-IR) spectroscopy. The adsorption kinetics of TA onto SMZ with CPB bilayer coverage (SMZ-CBC) followed a pseudo-second-order model. The equilibrium adsorption data of TA onto SMZ-CBC were well represented by Langmuir, Redlich-Peterson and Sips isotherm models. The calculated thermodynamic parameters indicated that TA adsorption onto SMZ-CBC was spontaneous and exothermic. The TA adsorption capacity for SMZ-CBC slightly decreased with increasing ionic strength but significantly increased with increasing Cu(II) concentration. The TA adsorption capacity for SMZ-CBC was relatively high at solution pH 4.0–7.0, and decreased with an increase in solution pH from 7.0 to 8.5. The mechanisms controlling TA adsorption onto SMZ-CBC at solution pH 5.5 include electrostatic attraction, hydrogen bonding and organic partitioning.

© 2011 Elsevier B.V. All rights reserved.

1. Introduction

Tannic acid (TA) is a component of natural organic matter (NOM) in surface and ground water, which is derived from the breakdown of plant biomass [1,2]. TA is also found in wastewater discharged from coir and cork process, plant medicine, paper and leather industries [2,3]. TA may cause a serious problem for drinking water production because TA can form carcinogenic disinfection by-products (DBPs) such as trihalomethanes (THMs) during chlorination process [1,2], which currently are regulated by the U.S. Environmental Protection Agency (EPA) under the Stage 1 Disinfectants and Disinfection By-Products (D/DBP) Rule [4]. In addition, as a water soluble polyphenolic compound, TA has toxicity for aquatic organisms such as algae, phytoplankton, fish and invertebrates [1]. Therefore, it is of great importance to remove TA from water and wastewater in terms of protecting human health and environment. There are various technologies to remove TA from water and wastewater, such as chemical oxidation, electrochemical process, coagulation, ultrafiltration, biological process and adsorption [1,5]. Among these technologies,

adsorption has been extensively developed to remove TA from water and wastewater [3]. Various adsorbents such as amino-functionalized magnetic mesoporous silica [1], bi-function resin [2], amino-functionalized magnetic nanoadsorbent [3], polymeric resins [6], cationic surfactant-modified bentonite clay [7], organically modified attapulgite clay [8], chitosan-montmorillonite [9], calcined and uncalcined hydrotalcites [10], activated carbon [11] and deacetylated konjac glucomannan [12] have been reported for removing TA from water and wastewater.

Zeolites are hydrated aluminosilicate minerals with a framework formed by tetrahedra of SiO_4 and AlO_4 containing water molecules, alkali and alkaline earth metals in their structural framework [13]. Since zeolites have a net permanent negative charge resulting from isomorphic substitution of Si^{4+} by Al^{3+}, cationic surfactants such as hexadecyltrimethylammonium bromide (HTAB) and cetylpyridinium bromide (CPB) are suitable for surface modification of zeolites [13–30]. The positive head groups of cationic surfactants readily exchange with the exchangeable cations on the external surface of zeolite, forming surfactant monolayers [25]. In properly chosen conditions, the loaded cationic surfactants on the external surface of zeolite form bilayers, where the upper layer is bound to the lower layer by the hydrophobic interaction between the tail groups of surfactants in both layers [20]. Surfactant-modified zeolites (SMZs) have been investigated as adsorbents for

removing various pollutants such as chromate [14–17], arsenate [18], phosphate [19], nitrate [20–22], phenol [24], 4-chlorophenol [24], volatile petroleum hydrocarbons [25], orange II [26], bisphenol A [27], fulvic acid (FA) [28], humic acid (HA) [29] and sodium dodecyl benzene sulfonate (SDBS) [30] from aqueous solution. However, to our knowledge, the use of SMZs as adsorbents to remove TA from aqueous solution has not been studied.

In this work, SMZs with various loadings of CPB were prepared and were used as adsorbents to remove TA from aqueous solution. The TA adsorption efficiencies for natural zeolite and various SMZs were compared. The effects of several experimental parameters such as contact time, initial adsorbate concentration, temperature, ionic strength, coexisting Cu(II) and solution pH on TA adsorption onto SMZ with CPB bilayer coverage were investigated. The effect of solution pH on TA adsorption onto SMZ with monolayer coverage was investigated. The experimental results were analyzed by kinetic and isotherm models. Thermodynamic parameters such as Gibbs free energy change (ΔG°), enthalpy change (ΔH°) and entropy change (ΔS°) were calculated. The adsorbents before and after adsorption were characterized by X-ray diffraction (XRD), field emission scanning electron microscope (FE-SEM), thermogravimetric analysis (TGA) and Fourier transform infrared (FT-IR) spectroscopy. The mechanisms for TA adsorption onto SMZs were also advised.

2. Materials and methods

2.1. Materials

Natural zeolite (NZ) originated from a mineral deposit in Jinyun County, Zhejiang Province, China, and it was crushed and sieved to obtain a particle size smaller than 0.075 mm. SMZs were prepared as follows. First, 18 g of natural zeolites and various volumes (72–324 mL) of CPB stock solutions with an initial concentration of 25 mmol/L were mixed on a shaker equipped with thermostat at 40 °C for 48 h. The mixtures were then centrifuged and the supernatants were removed. The residual concentrations of CPB in the supernatants were measured by TU-1901 UV/Vis spectrophotometer (Beijing Purkinje General Instrument Co., Ltd., China) with detecting wavelength at 259 nm. The amounts of CPB loaded onto natural zeolites were calculated based on the difference between the initial and residual concentrations of CPB in the solution. The concentrations of Na^+, K^+, Mg^{2+} and Ca^{2+} in the supernatants were measured by an Optima 2100 DV inductively coupled plasma atomic emission spectroscopy (PerkinElmer, USA), which were used to calculate the total equivalent amounts of cations exchanged from natural zeolites. After that, the resulting SMZs were washed with distilled water until no Br^- was detected by $AgNO_3$ solution and finally dried in an oven at 50 °C. Hereafter, the zeolites modified with 72, 108, 144, 180, 216 and 324 mL of CPB solutions were named as SMZ1, SMZ2, SMZ3, SMZ4, SMZ5 and SMZ6, respectively.

2.2. Adsorption experiment

All batch adsorption experiments were performed in conical flasks stirred on a shaker equipped with thermostat at 150 rpm.

2.2.1. Comparison of TA adsorption by natural zeolite and various SMZs

Adsorption experiment was carried out by shaking 50 mg of adsorbents in 100 mL of TA solutions with an initial concentration of 100 mg/L (pH 5.5) at 30 °C. After 24 h, the aqueous samples were filtrated, the concentrations of TA in the filtrates were determined using a TU-1901 UV/Vis spectrophotometer (Beijing Purkinje General Instrument Co., Ltd., China) with detecting wavelength at 278 nm, and the concentrations of bromide in the filtrates were

determined using an ICS-900 ion chromatograph (Dionex Corporation, USA).

2.2.2. Adsorption kinetics

Adsorption kinetics study was carried out by shaking 50 mg of SMZ in 100 mL of TA solutions with an initial concentration of 50 mg/L (pH 5.5) at 30 °C. After pre-defined contact time, the aqueous sample was filtered, and the concentration of TA in the filtrate was spectrophotometrically determined.

2.2.3. Adsorption isotherm

Adsorption isotherm study was carried out by shaking 50 mg of SMZ in 100 mL of TA solutions with initial concentrations ranging from 15 to 100 mg/L (pH 5.5) at 30 °C. After 24 h, the aqueous samples were filtrated, and the concentrations of TA in the filtrates were spectrophotometrically determined.

2.2.4. Thermodynamics

Thermodynamic study was carried out by shaking 50 mg of SMZ in 100 mL of TA solutions with initial concentrations ranging from 30 to 60 mg/L (pH 5.5) at 30 °C, 35 °C, 40 °C and 50 °C. After 24 h, the aqueous samples were filtrated, and the concentrations of TA in the filtrates were spectrophotometrically determined.

2.2.5. Effect of ionic strength

Adsorption experiment was carried out by shaking 50 mg of SMZ in 100 mL of solutions with different concentrations of NaCl (0, 0.025, 0.05, 0.1, 0.15, 0.2, 0.4, 0.6 and 0.8 mol/L) and an initial TA concentration of 50 mg/L (pH 5.5) at 30 °C. After 24 h, the aqueous samples were filtrated, and the concentrations of TA in the filtrates were spectrophotometrically determined.

2.2.6. Effect of coexisting Cu(II)

Adsorption experiment was carried out by shaking 50 mg of SMZ in 100 mL of solutions with different concentrations of Cu(II) (0, 1, 2, 4, 6, 8 and 10 mg/L) and an initial TA concentration of 100 mg/L (pH 5.5) at 30 °C. After 24 h, the aqueous samples were filtrated, and the concentrations of TA in the filtrates were spectrophotometrically determined.

2.2.7. Effect of solution pH

The effect of solution pH on TA adsorption was investigated by adjusting TA solutions (20 and 50 mg/L) to different pH values (4.0, 4.5, 5.0, 5.5, 6.0, 6.5, 7.0, 7.5, 8.0 and 8.5) and shaking 50 mg of SMZ in 100 mL of TA solutions at 30 °C. After 24 h, the aqueous samples were filtrated, and the concentrations of TA in the filtrates were spectrophotometrically determined.

2.2.8. Characterization of adsorbents before and after adsorption of TA

The adsorbents before and after adsorption of TA at solution pH 5.5 were characterized by TGA, XRD, FE-SEM and FT-IR spectroscopy. Power XRD patterns of solid samples were obtained using an X'Pert PRO X-ray diffractometer with Cu Kα radiation (PANalytical, The Netherlands) operating at 40 kV and 40 mA. The surfaces of solid samples were examined using a JSM-7500F FE-SEM (JEOL Ltd., Japan). TGA of solid samples was conducted using a SDT-Q600 simultaneous thermal analyzer (TA Instruments Inc., USA). The solid samples were heated from 50 to 600 °C at a heating rate of 10 °C/min under a nitrogen flow rate of 100 mL/min. FT-IR spectra of solid samples were recorded at 400–4000 cm^{-1} using a Nicolet 5700 model FT-IR spectrometer (Thermo Nicolet Corporation, USA) with a resolution of 2 cm^{-1}.
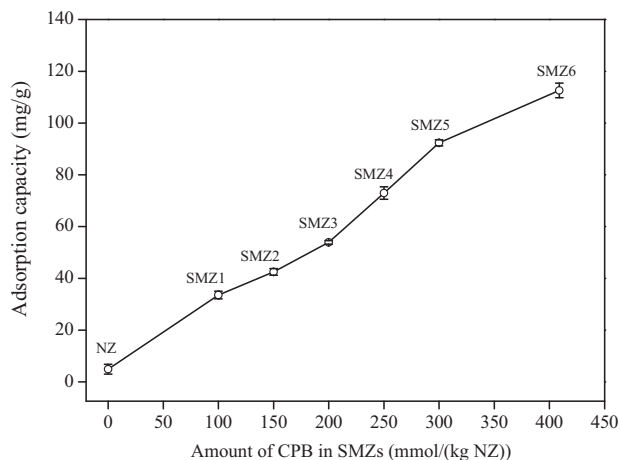
Fig. 1. Comparison of adsorption efficiencies for natural zeolite and various SMZs.

3. Results and discussion

3.1. Amount of CPB in SMZs

The CPB loading amounts of SMZ1, SMZ2, SMZ3, SMZ4, SMZ5 and SMZ6 were found to be 100, 150, 200, 250, 300 and 409 mmol/(kg NZ), respectively [31]. SMZ1 and SMZ2 had CPB monolayer coverage, SMZ3, SMZ4 and SMZ5 had CPB patchy bilayer coverage, and SMZ6 had CPB bilayer coverage [31].

3.2. Comparison of TA adsorption by natural zeolite and various SMZs

The comparison of TA adsorption efficiencies for natural zeolite and various SMZs at solution pH 5.5 is shown in Fig. 1. Results showed that the natural zeolite had little affinity for TA in aqueous solution. However, the SMZ presented higher TA adsorption efficiency than the natural zeolite. Furthermore, the TA adsorption efficiency was in the order of SMZ6 > SMZ5 > SMZ4 > SMZ3 > SMZ2 > SMZ1, indicating that the SMZ with higher loading amount of CPB exhibited higher TA adsorption efficiency and the SMZ with the maximum loading amount of CPB was the most efficient adsorbent for the removal of TA from aqueous solution.

TA molecules contain hydrophilic phenolic groups and hydrophobic aromatic groups [8], and they exist in aqueous solution as both unionized and ionized forms at pH 5.5 [9]. The low adsorption efficiency of TA onto natural zeolite may be attributed to two reasons. Since natural zeolites possess net negative structural charges on their frameworks that are balanced by inorganic counterions such as Na$^+$, K$^+$, Ca^{2+} and Mg^{2+} [13], they obviously cannot remove the negatively charged TA molecules from aqueous solution through anion exchange and electrostatic attraction. The adsorption of TA onto natural zeolites is negligible also because of the strong dipole interaction between zeolite and water, which exclude organic solutes from this portion of the zeolite [28,30]. The high adsorption efficiency of TA onto SMZ is attributed to its CPB layers.

For SMZ1 and SMZ2, the loaded CPB molecules on the zeolite surface formed monolayers [31]. This monolayer formation does not cause a charge reversal on the external surface of zeolite from negative to positive [23]. Therefore, the SMZ with CPB monolayer coverage is obviously unable to remove the negatively charged TA molecules from aqueous solution through anion exchange and electrostatic attraction. This conclusion is supported by the fact that negligible bromide was desorbed from SMZ1 and SMZ2 after the adsorption of TA. In previous literatures, the mechanisms control-

ling organic solutes such as fulvic acid (FA) and sodium dodecyl benzene sulfonate (SDBS) adsorption onto SMZ with HTAB monolayer coverage have been proposed [28,30]. FA adsorption onto SMZ with HTAB monolayer coverage is largely due to hydrophobic interaction and hydrogen bonding [28]. Hydrophobic interaction and hydrogen bonding are suggested to be responsible for SDBS adsorption onto SMZ with HTAB monolayer coverage [30]. Based on the reports in the previous literatures [28,30], it is postulated that the adsorption of TA onto SMZ with CPB monolayer coverage is attributed to: (i) hydrogen bonding between the nitrogen atoms of CPB monolayers and the phenolic groups of TA molecules; and (ii) hydrophobic interaction between the hydrophobic tails of CPB monolayers and the hydrophobic functional groups of TA molecules.

For SMZ6, the loaded CPB molecules on the zeolite surface formed bilayers [31]. This bilayer formation results in a charge reversal on the external surface of zeolite from negative to positive and the positively charged outward-pointing head groups of CPB bilayers are balanced by counterions bromide [17,31]. Therefore, it is postulated that the SMZ with CPB bilayer coverage can remove the negatively charged TA molecules from aqueous solution through anion exchange and electrostatic attraction. In order to confirm this mechanism, the concentration of desorbed bromide from SMZ6 after the adsorption of TA was analyzed. When the TA adsorption capacity for SMZ6 was 66 mmol/kg, the amount of desorbed bromide from SMZ6 was found to be 171 mmol/kg. This confirms that the mechanisms controlling the adsorption of TA onto SMZ with CPB bilayer coverage include anion exchange and electrostatic attraction. Although the mole ratio of the amount of desorbed bromide to the amount of adsorbed TA is 2.6, we cannot make a conclusion that the anion exchange is the only mechanism controlling the adsorption of TA onto SMZ with CPB bilayer coverage considering that every unit of completely ionized TA molecule carries approximate four negative charges [9]. Hydrogen bonding may also play a role in the adsorption of TA onto SMZ with CPB bilayer coverage because the phenolic groups of TA molecules may act as hydrogen bonding donators and the nitrogen atoms of CPB bilayers may act as hydrogen bonding acceptors. In addition, the adsorption of TA onto SMZ with CPB bilayer coverage may involve partitioning of TA molecules into CPB bilayers, and this mechanism is of London-Van der Waals type [27].

For SMZ3, SMZ4 and SMZ5, the loaded CPB molecules on the zeolite surface formed patchy bilayers, that is, CPB molecules in these SMZs existed as both monolayers and bilayers. Therefore, it is postulated that the adsorption of TA onto SMZ with patchy bilayer coverage is attributed to: (i) electrostatic interaction between the positively charged outward-pointing head groups of CPB bilayers and the negatively charged TA molecules; (ii) hydrogen bonding between the nitrogen atoms of CPB layers (monolayers and bilayers) and the phenolic groups of TA molecules; (iii) partitioning of TA molecules into CPB bilayers; and (iv) hydrophobic interaction between the hydrophobic tails of CPB monolayers and the hydrophobic functional groups of TA molecules.

3.3. Adsorption kinetics

The adsorption of TA onto SMZ6 (SMZ with CPB bilayer coverage) as a function of contact time at solution pH 5.5 is shown in Fig. 2. Results showed that the rate of adsorption was rapid at the beginning and gradually decreased with increasing contact time until equilibrium was attained. Two widely used kinetic models, pseudo-first-order and pseudo-second-order kinetic models, were employed to interpret the kinetics results. The linearized form of pseudo-first-order kinetic model is given as follows [3]:
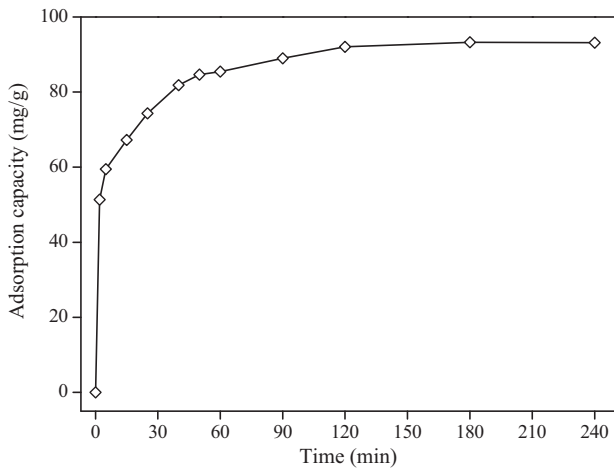
$$\ln(q_e - q_t) = \ln(q_e) - k_1 t \tag{1}$$

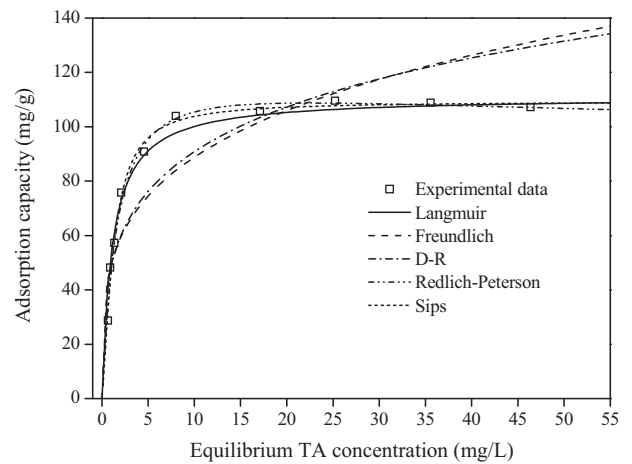**Fig. 2.** Effect of contact time on TA adsorption onto SMZ6.

Fig. 3. Adsorption isotherm of TA onto SMZ6.

where q_e (mg/g) and q_t (mg/g) are the TA adsorption capacities for SMZ6 at equilibrium and at any time t (min), respectively. k_1 (1/min) is the rate constant of pseudo-first-order kinetic model. The linear plot of $\ln(q_e - q_t)$ versus t was used to calculate the rate constant k_1, the equilibrium adsorption capacity q_e, and the determination coefficient R^2, and the results are given in Table 1. Although the R^2 value obtained was relatively high ($R^2 = 0.985$), the calculated q_e value did not agree with the experimental one. This suggests that the pseudo-first-order kinetic model is not appropriate to represent the adsorption kinetics data of TA onto SMZ6. The linearized form of pseudo-second-order kinetic model is given as follows [3]:

$$\frac{t}{q_t} = \frac{1}{k_2 q_e^2} + \frac{t}{q_e} \tag{2}$$

where k_2 (g/mg min) is the rate constant of pseudo-second-order kinetic model. The values of equilibrium adsorption capacity q_e and rate constant k_2, calculated from the intercept and the slope of the linear plot of t/q_t versus t, along with the value of determination coefficient R^2, are listed in Table 1. The R^2 value obtained was very high ($R^2 > 0.999$), and the calculated q_e value was in good agreement with the experimental one, suggesting the applicability of the pseudo-second-order kinetic model to describe the adsorption kinetics data of TA onto SMZ6.

3.4. Adsorption isotherm

The adsorption isotherm of TA onto SMZ6 (SMZ with CPB bilayer coverage) at 30 °C and solution pH 5.5 is shown in Fig. 3. Results showed that the TA adsorption capacity increased with increasing the equilibrium TA concentration until equilibrium was reached. Two-parameter isotherm models (Langmuir, Freundlich and Dubinin-Radushkevish (D-R)) and three-parameter isotherm models (Redlich-Peterson and Sips) were used to fit the experimental data. The linearized form of Langmuir isotherm model can be written as [32]:

$$\frac{C_e}{q_e} = \frac{1}{q_{max} K_L} + \frac{C_e}{q_{max}} \tag{3}$$

where C_e (mg/L) is the equilibrium concentration of TA in solution. q_e (mg/g) is the TA adsorption capacity for SMZ6 at equilibrium. q_{max} (mg/g) is the maximum monolayer TA adsorption capacity for SMZ6. K_L (L/mg) is the Langmuir isotherm constant related to the free energy of adsorption. The values of q_{max} and K_L can be calculated from the intercept and the slope of the straight line of the linearized form of the Langmuir isotherm. The essential characteristics of the Langmuir isotherm can be expressed in terms of a dimensionless constant separation factor, R_L, which is defined as follows [32]:

$$R_L = \frac{1}{1 + K_L C_0} \tag{4}$$

where C_0 (mg/L) is the initial concentration of TA in solution. The adsorption is considered favorable when $0 < R_L < 1$ [32].

The linearized form of Freundlich isotherm model can be written as [32]:

$$\ln(q_e) = \ln(K_F) + \frac{1}{n} \ln(C_e) \tag{5}$$

where K_F ((mg/g)(L/mg)$^{1/n}$) and $1/n$ are the Freundlich constants which are related to the adsorption capacity and adsorption intensity, respectively. The values of K_F and $1/n$ can be calculated from the intercept and the slope of the straight line of the linearized form of the Freundlich isotherm.

The linearized form of D-R isotherm model can be written as [33]:

$$\ln(q_e) = \ln(q_{max}) - K_D \left[RT \ln \left(1 + \frac{1}{C_e} \right) \right]^2 \tag{6}$$

where C_e (mol/L) is the equilibrium concentration of TA in solution. q_e (mol/g) is the TA adsorption capacity for SMZ6 at equilibrium. q_{max} (mol/g) is the maximum TA adsorption capacity for SMZ6. K_D (mol^2/kJ^2) is the D-R isotherm constant related to the free energy of adsorption. R (8.314 J/mol K) is the gas constant. T (K) is the absolute temperature. The values of K_D and q_{max} can be calculated from the intercept and the slope of the straight line of the linearized form of the D-R isotherm.

Table 1
Pseudo-first-order and pseudo-second-order rate constants for TA adsorption onto SMZ6.

C_0 (mg/L)	$q_{e,exp}$ (mg/g)	Pseudo-first-order model			Pseudo-second-order model		
		k_1 (1/min)	$q_{e,cal}$ (mg/g)	R^2	k_2 (g/mg min)	$q_{e,cal}$ (mg/g)	R^2
50	93.3	0.0278	39.5	0.985	0.00202	95.2	1.00

Table 2
Isotherm parameters for TA adsorption onto SMZ6.

Langmuir	q_{max} (mg/g)	K_L (L/mg)	R^2	
	111	0.918	0.999	
Freundlich	K_F ((mg/g)(L/mg)$^{1/n}$)	$1/n$	R^2	
	49.5	0.254	0.779	
D-R	q_{max} (mg/g)	K_D (mol^2/kJ^2)	R^2	
	400	0.00161	0.809	
Redlich-Peterson	K_R (L/g)	α_R ((L/mg)$^{\beta}$)	β	R^2
	71.0	0.485	1.07	0.987
Sips	q_{axm} (mg/g)	K_s ((L/mg)^m)	m	R^2
	109	0.765	1.39	0.991

The Redlich-Peterson isotherm model is used as a compromise between Langmuir and Freundlich isotherm models [34,35]. The non-linearized form of Redlich-Peterson isotherm model can be given as follows [34,35]:

$$q_e = \frac{K_R C_e}{1 + \alpha_R C_e^{\beta}} \tag{7}$$

where K_R (L/g) and α_R ((L/mg)$^{\beta}$) are Redlich-Peterson isotherm constants. β is the exponent which lies between 0 and 1 and can characterize the adsorption isotherm. If $\beta = 1$, Eq. (7) reduces to the Langmuir isotherm model, and if $\beta = 0$, Eq. (7) reduces to the linear isotherm model [34]. The values of K_R, α_R and β can be obtained by nonlinear regression method.

The Sips isotherm model is obtained by introducing a power law expression of the Freundlich isotherm into the Langmuir isotherm [36]. The non-linearized form of Sips isotherm model can be given as follows [36]:

$$q_e = \frac{q_{max} K_s C_e^m}{1 + K_s C_e^m} \tag{8}$$

where q_{max} (mg/g) is the maximum monolayer TA adsorption capacity for SMZ6. K_s ((L/mg)^m) is the Sips isotherm constant representing the energy of adsorption. m is the empirical constant. The values of K_s, q_{max} and m can be obtained by nonlinear regression method.

The parameters of Langmuir, Freundlich, D-R, Redlich-Peterson and Sips isotherm models for TA adsorption onto SMZ6, along with the values of determination coefficient (R^2), are given in Table 2. The values of R^2 for the Freundlich and D-R isotherm models were low, indicating that the equilibrium adsorption of TA onto SMZ6 cannot be represented appropriately by these two isotherm models. The values of R^2 for the Langmuir, Redlich-Peterson and Sips isotherm models were high, indicating that the equilibrium data for the adsorption of TA onto SMZ6 can be well represented by these three isotherm models. The value of β for the Redlich-Peterson isotherm was close to unity, which means that the isotherm conforms to the Langmuir isotherm model better than the Freundlich isotherm model. Based on the fact that the experimental data fits well with the Langmuir isotherm model, it can be concluded that the adsorption of TA onto SMZ6 takes place as monolayer adsorption and the surface of SMZ6 is homogenous in adsorption affinity. The predicted maximum monolayer TA adsorption capacity for SMZ6 derived from Langmuir isotherm was found to be 111 mg/g, which is comparable to that of cationic surfactant-modified bentonite clay (119 mg/g) [7]. The values of R_L obtained in this study were between 0.0108 and 0.0667, indicating that the adsorption of TA onto SMZ6 is favorable. According to the Sips isotherm model, the predicted maximum monolayer TA adsorption capacity was
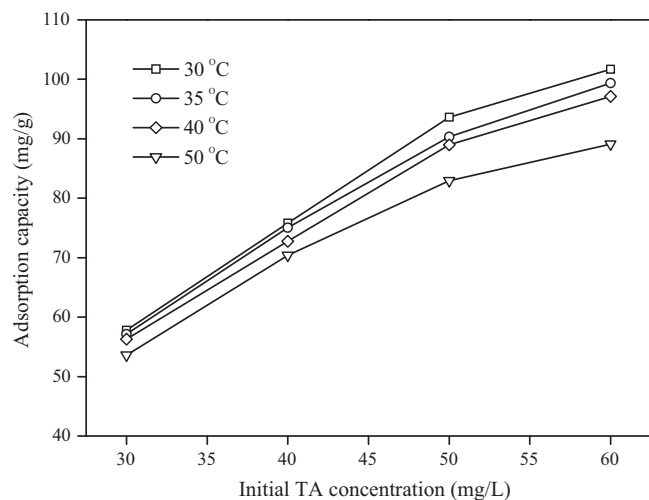
Fig. 4. Effect of temperature on TA adsorption onto SMZ6.

determined to be 109 mg/g, which is very close to that derived from Langmuir isotherm.

3.5. Thermodynamics

The adsorption of TA onto SMZ6 (SMZ with CPB bilayer coverage) as a function of temperature at solution pH 5.5 is shown in Fig. 4. Results showed that the TA adsorption capacity for SMZ6 decreased with increasing temperature, which indicates that the adsorption of TA onto SMZ6 is favored at lower temperarture. Similar influence of temperature on TA adsorption was observed for cationic surfactant-modified bentonite clay [7]. The above experimental data were evaluated by Langmuir isotherm model. The obtained results are listed in Table 3. The values of K_L for the Langmuir isotherm at 30 °C, 35 °C, 40 °C and 50 °C were used to calculate thermodynamic parameters such as Gibbs free energy change ($\Delta G°$), enthalpy change ($\Delta H°$) and entropy change ($\Delta S°$) using following equations [35,36]:

$$\Delta G° = -RT \ln K_L \tag{9}$$

$$\ln K_L = \frac{\Delta S°}{R} - \frac{\Delta H°}{RT} \tag{10}$$

where K_L (L/mol) is the Langmuir constant. R (8.314 J/mol K) is the gas constant. T (K) is the absolute temperature. The values of $\Delta H°$ and $\Delta S°$ can be calculated from the intercept and the slope of the linear plot of $\ln K_L$ versus $1/T$. The obtained values of thermodynamic parameters for TA adsorption onto SMZ6 are given in Table 4. The negative values of $\Delta G°$ suggest the feasibility of the adsorption of TA onto SMZ6 and the spontaneous nature of the

Table 3
Langmuir isotherm parameters for TA adsorption onto SMZ6 at different temperatures.

Temperature	30 °C	35 °C	40 °C	50 °C
q_{max} (mg/g)	113	112	113	106
K_L (L/mg)	1.08	0.788	0.547	0.375
R^2	0.999	0.999	0.997	0.995

Table 4
Thermodynamic parameters for TA adsorption onto SMZ6.

$\Delta H°$ (kJ/mol)	$\Delta S°$ (J/mol K)	$\Delta G°$ (kJ/mol)				R^2
		30 °C	35 °C	40 °C	50 °C	
−43.2	−23.2	−36.3	−36.1	−35.8	−35.9	0.981

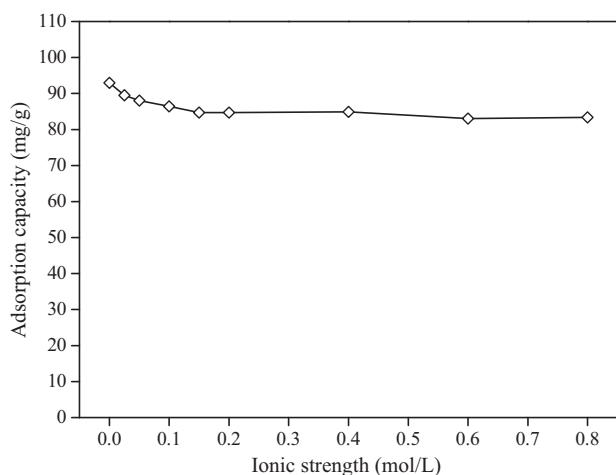**Fig. 5.** Effect of ionic strength on TA adsorption onto SMZ6.

Fig. 6. Effect of Cu(II) on TA adsorption onto SMZ6.

adsorption process. In general, the value of ΔG° for physisorption is between -20 and $0\,kJ/mol$, and that for chemisorption is between -400 and $-80\,kJ/mol$ [35]. The values of ΔG° obtained in this study were in the range of neither physisorption nor chemisorption, indicating that the adsorption of TA onto SMZ6 involves the other adsorption process such as ion exchange. This conclusion confirms that the mechanisms controlling the adsorption of TA onto SMZ6 at solution pH 5.5 include anion exchange and electrostatic attraction. The negative value of ΔH° indicates that the adsorption process is exothermic in nature. The energy of adsorption from different forces were as follows: Van der Waals forces $4–10\,kJ/mol$, hydrophobic bond forces about $5\,kJ/mol$, hydrogen bond forces $2–40\,kJ/mol$, coordination exchange about $40\,kJ/mol$, dipole bond forces $2–29\,kJ/mol$ and chemical bond forces $>60\,kJ/mol$ [8]. The absolute value of ΔH° was $43.2\,kJ/mol$, indicating that hydrogen bonding and organic partitioning are also of importance to the adsorption process in addition to electrostatic attraction. The negative value of ΔS° shows a decrease in randomness at the solid/liquid interface during the adsorption process.

3.6. Effect of ionic strength

The adsorption of TA onto SMZ6 (SMZ with CPB bilayer coverage) as a function of ionic strength at solution pH 5.5 is shown in Fig. 5. The presence of electrolytes such as NaCl in aqueous solution had a slight negative effect on TA adsorption onto SMZ6. When the ionic strength of the aqueous solution increased from 0 to 0.8 mol/L, the TA adsorption capacity decreased from 93 to 83 mg/g. This result suggests that SMZ with CPB bilayer coverage is effective in removing TA from water or wastewater containing salt. If electrostatic attraction is the main adsorption mechanism, the ionic strength should have a significant negative effect on the adsorption process [37,38]. The slight negative effect of ionic strength on TA adsorption onto SMZ6 at solution pH 5.5 confirms that the electrostatic attraction is not the only mechanism for the adsorption process and the electrostatic attraction together with the other mechanisms such as hydrogen bonding and organic partitioning control the adsorption process. The slight decrease of TA adsorption capacity after NaCl addition may be explained as follows. On one hand, TA adsorption onto SMZ6 may be reduced by the chloride ions due to the competition between the chloride ions and the ionized TA ions for the adsorption sites on the surface of the adsorbent. On the other hand, TA adsorption onto SMZ6 may be enhanced by the sodium ions due to the weakening of the repulsive interaction between adsorbed TA molecules on the surface of the adsorbent and TA molecules in solution [1]. The decreased TA adsorption
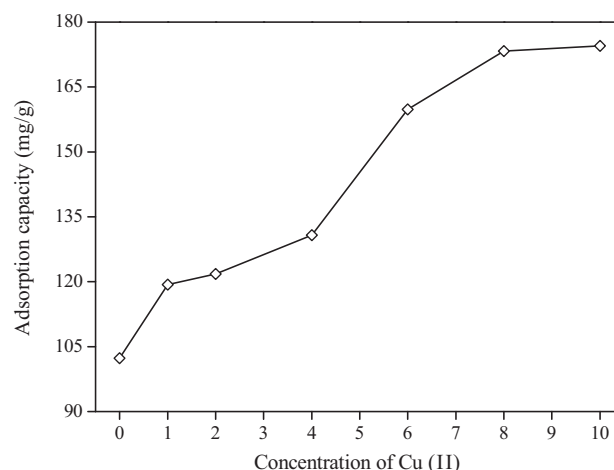
caused by the chloride ions may be partially counteracted by the increased TA adsorption caused by the sodium ions, resulting in that TA adsorption is slightly reduced by the ionic strength of the aqueous solution.

3.7. Effect of coexisting Cu(II)

Since heavy metal ions may be present in water or wastewater, it is necessary to study the effects of heavy metal ions on the adsorption of TA onto SMZ. The adsorption of TA onto SMZ6 (SMZ with CPB bilayer coverage) as a function of coexisting Cu(II) at solution pH 5.5 is shown in Fig. 6. The presence of Cu(II) in aqueous solution led to markedly enhanced TA adsorption onto SMZ6. When the initial concentration of Cu(II) in aqueous solution increased from 0 to 10 mg/L, the TA adsorption capacity for SMZ6 increased from 102 to 175 mg/g. Similar influence of coexisting Cu(II) on TA adsorption was observed for a new bi-function resin WJN-09 [2]. This is possible because average molecule diameter of TA increases dramatically when Cu(II) is added into aqueous solution due to complex compounds formed between Cu(II) and TA [2], which may result in that more TA molecules are adsorbed by the same amounts of the adsorption sites on the surface of SMZ6. In addition, coexisting Cu(II) in solution may neutralize the repulsive force between TA molecules in aqueous solution and TA molecules adsorbed on the surface of the adsorbent, which may also favor the adsorption of TA onto SMZ6.

3.8. Effect of solution pH

The pH of an aqueous solution is an important variable that governs the adsorption of TA onto adsorbents [1,7]. The adsorption of TA onto SMZ6 (SMZ with CPB bilayer coverage) as a function of solution pH is shown in Fig. 7. Results showed that the TA adsorption capacity for SMZ6 was relatively high at solution pH 4.0–7.0, and decreased with increasing solution pH from 7.0 to 8.5. This observation is explained as follows. TA is a weak organic acid, and its ionization is strongly dependent on solution pH [9]. At solution pH below 4.5, TA molecule is present in a neutral form [9]. The adsorption of unionized TA onto the positively charged surface of SMZ6 is unlikely to be driven by the electrostatic attraction. Therefore, the hydrogen bonding and organic partitioning are responsible for the adsorption of TA onto SMZ6 at solution pH 4.0–4.5. TA molecules are ionized at solution pH above 4.5, and they are almost completely ionized at solution pH 7.0 [9]. Therefore, the electrostatic attraction together with the hydrogen bonding and organic partitioning are responsible for the adsorption of TA onto SMZ6 at
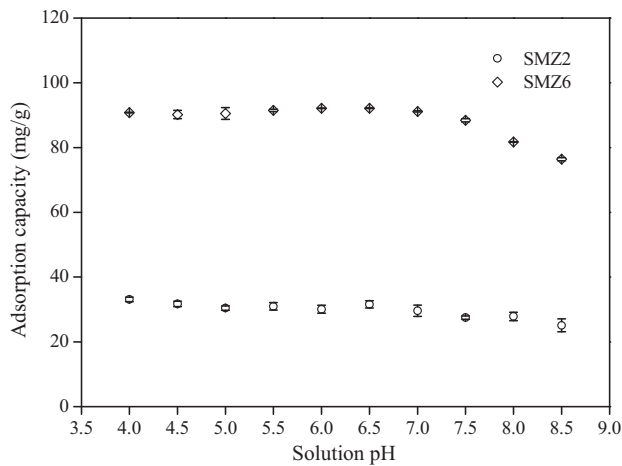
Fig. 7. Effect of solution pH on TA adsorption onto SMZ2 and SMZ6.

Fig. 8. XRD patterns of SMZ6 and TA-adsorbed SMZ6.

solution pH 4.5–7.0. The increase of solution pH from 4.5 to 7.0 leads to the decreased hydrogen bonding between TA and SMZ6 but the increased electrostatic attraction between TA and SMZ6. The former is counteracted by the latter, resulting in that the adsorption of TA onto SMZ6 is slightly influenced by solution pH at 4.5–7.0. At solution pH above 7.0, completely ionized TA molecules cannot provide hydroxyl hydrogen atom to nitrogen atom of CPB bilayer of SMZ6 to form hydrogen bonding. In this case, the electrostatic attraction plays an important role in the adsorption of TA onto SMZ6. The increase of solution pH from 7.0 to 8.5 leads to the increase of the competitions between the hydroxyl ion and the ionized TA molecule for the same positively charged adsorption sites on the surface of SMZ6, which causes a decreased TA adsorption capacity. The adsorption of TA onto SMZ2 (SMZ with CPB mono-layer coverage) as a function of solution pH is also shown in Fig. 7. Results showed that the TA adsorption capacity for SMZ2 remained nearly constant at solution pH 4.0–7.0. In addition, the TA adsorption capacity for SMZ2 at solution pH 4.5–7.0 was slightly higher than that at solution pH 7.5–8.5. As stated earlier, the adsorption of TA onto SMZ2 may involve the hydrogen bonding and hydrophobic interaction. The strength of the hydrophobic interaction is not appreciably influenced by the solution pH [39]. If the hydrogen bonding plays an important role in the adsorption of TA onto SMZ2, the TA adsorption capacity is expected to decrease with increasing solution pH from 4.5 to 7.0 because the increase of solution pH from 4.5 to 7.0 results in the decreased hydrogen bonding. The fact that the TA adsorption capacity is slightly influenced by solution pH at 4.5–7.0 indicates that the hydrogen bonding is unlikely to play an important role in the adsorption of TA onto SMZ2. Therefore,
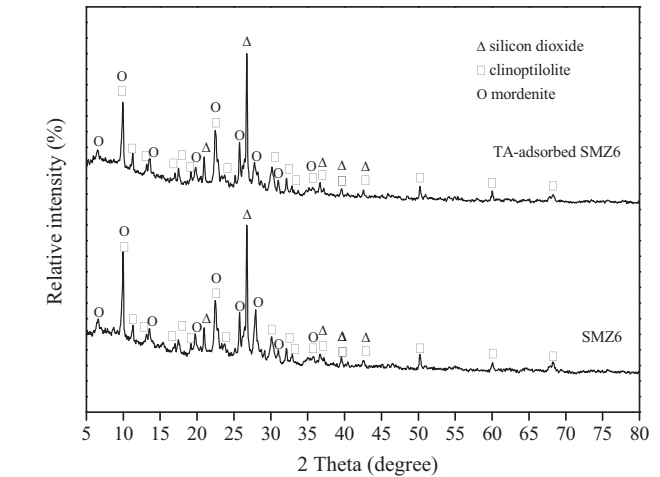
the hydrophobic interaction is the main mechanism controlling the adsorption of TA onto SMZ2.

3.9. Characterization of adsorbents before and after adsorption of TA

Fig. 8 shows the XRD patterns of SMZ6 and TA-adsorbed SMZ6. The XRD pattern in Fig. 8 confirmed the existence of clinoptilo-lite, mordenite and quartz in SMZ6 and TA-adsorbed SMZ6. The major X-ray peaks of SMZ6 were very close to those of TA-adsorbed SMZ6 which indicates that the crystalline nature of the zeolite in SMZ6 remains intact after the adsorption of TA onto SMZ6. The peak at 2θ of 9.98 for TA-adsorbed SMZ6 has lower relative inten-sity than that for SMZ6, which results from the adsorption of TA onto SMZ6.

Fig. 9 shows the FE-SEM images of SMZ6 and TA-adsorbed SMZ6. Our previous study has shown that the natural zeolite has drusy tex-ture with high microporosity, developed crystalline tabular habits and conglomerates of compact crystals [29]. The morphological dif-ference between SMZ6 and natural zeolite was observable. After the loading of CPB onto natural zeolite, the surfaces of the zeolite crystals were covered with an organic layer, but the edges of the zeolite crystals did not completely disappear (Fig. 9(a)). The surface morphology of TA-adsorbed SMZ6 was different from that of SMZ6. After the adsorption of TA onto SMZ6, the surface of SMZ6 was fully covered with an organic layer, and the edges of the zeolite crystals completely disappeared (Fig. 9(b)). These results confirm that the TA molecules have been adsorbed onto the surface of SMZ6 after the contact of SMZ6 with TA solution.
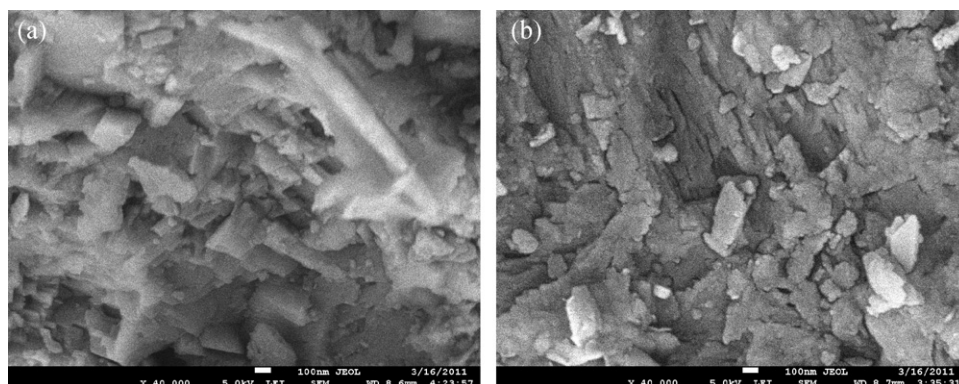

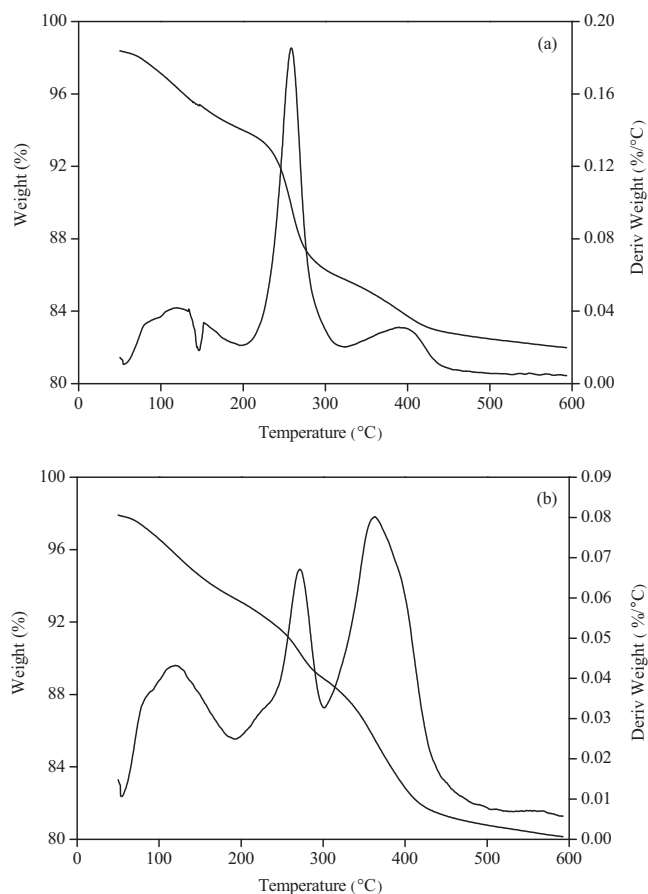**Fig. 9.** FE-SEM images of SMZ6 and TA-adsorbed SMZ6.

Fig. 10. TGA results of SMZ6 and TA-adsorbed SMZ6.

The thermal stability of organoclays and SMZs with different HTAB coverage types as well as the packing arrangement of cationic surfactant within the organoclays and SMZs at an elevated temperature had been determined by TGA [15,20,40,41]. However, to our best knowledge, no information about the thermal characterization of SMZs with CPB bilayer coverage is available in previous literatures. The TGA curves for SMZ6 are shown in Fig. 10(a). In Fig. 10(a), there were several mass loss steps observed. The mass

loss below 200 °C is attributed to the unbounded and physically adsorbed water [15,20]. The mass loss between 200 and 600 °C is attributed to the decomposition of CPB molecules within the SMZ6. The total mass loss due to CPB molecules decomposition was found to be 12.0%. The CPB loading amount of SMZ6 as calculated from the TGA data was 396 mmol/(kg NZ), which basically accords with that reported elsewhere (409 mmol/(kg NZ)) [31]. Two derivative curve peaks between 200 and 600 °C for SMZ6 were observed at 259 °C and 390 °C. The TGA curves for TA-adsorbed SMZ6 are shown in Fig. 10(b). In Fig. 10(b), there were several mass lost steps observed. The mass loss below 200 °C is attributed to the unbounded and physically adsorbed water [15,20]. The mass loss between 200 and 600 °C is attributed to the decomposition of organic molecules within the TA-adsorbed SMZ6. The total mass loss due to organic molecules decomposition was found to be 13.0%. Two derivative curve peaks between 200 and 600 °C for TA-adsorbed SMZ6 were observed at 272 °C and 363 °C. The total mass loss between 200 and 600 °C for TA-adsorbed SMZ6 was higher than that for SMZ6, and the positions and intensities of the two derivative curve peaks between 200 and 600 °C for TA-adsorbed SMZ6 were different from those for SMZ6, confirming the adsorption of TA onto SMZ6.

Fig. 11 shows the FT-IR spectra of SMZ6 and TA-adsorbed SMZ6. The FT-IR spectra of SMZ6 and TA-adsorbed SMZ6 showed two pronounced characteristic peaks (2800–3000 cm^{-1}), which are attributed to symmetric and asymmetric stretching vibrations of $-CH_2$ group of CPB molecule [31]. Two new peaks at 1714 cm^{-1} and 1319 cm^{-1} (assigned to C=O stretching vibrations and O−H inplane deformation of polyphenols, respectively [42,43]) were observed in the spectrum of TA-adsorbed SMZ6 as compared to that of SMZ6, confirming the adsorption of TA onto SMZ6. In general, the frequency of $-CH_2$ stretching vibration is highly sensitive to the gauche/trans conformer ratio and the packing density of alkyl chains [40,44]. Band shifts to higher wavenumber are characteristic of disorder gauche conformations, whereas band shifts to lower wavenumber are characteristic of highly ordered all-trans conformations [41,44]. In addition, shifts or changes of FT-IR characteristic peaks of functional groups in adsorbent and adsorbate will indicate interactions between these functional groups [45,46]. After the adsorption of TA onto SMZ6, the characteristic peak representing the asymmetric CH$_2$-stretching vibration slightly shifted from 2920 to 2924 cm^{-1}. This indicates that CPB molecules in TA-adsorbed SMZ6 have more disordered conformations than those in SMZ6, and there are interactions of TA molecules with alkyl chains of CPB
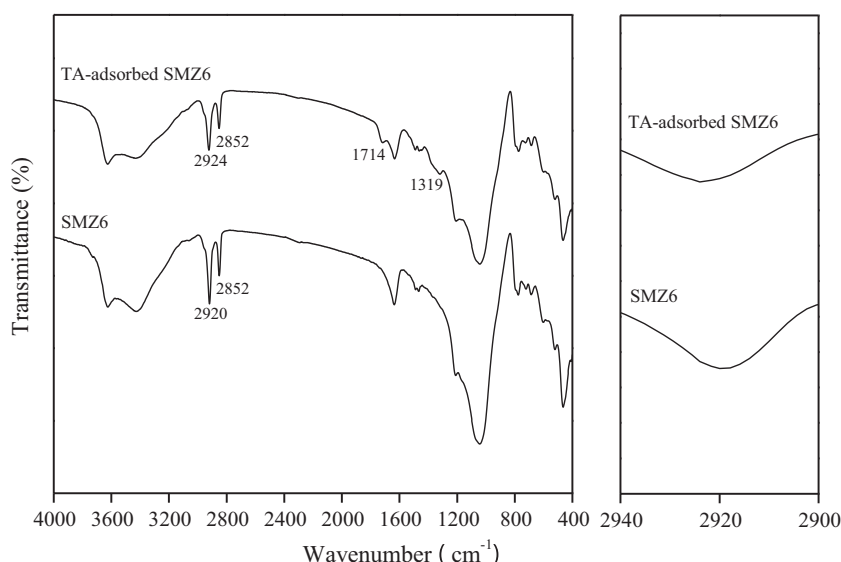

Fig. 11. FT-IR spectra of SMZ6 and TA-adsorbed SMZ6.

molecules through Van der Waals forces. This conclusion confirms that the mechanisms controlling the adsorption of TA onto SMZ6 at solution pH 5.5 include organic partitioning.

3.10. Proposed mechanisms

Taking all the results that have been discussed above into account, we propose that the main mechanism controlling the adsorption of TA onto SMZ with CPB monolayer coverage is the hydrophobic interaction; the mechanisms controlling the adsorption of TA onto SMZ with CPB bilayer coverage at solution pH 5.5 include the electrostatic attraction, hydrogen bonding and organic partitioning; and the mechanisms controlling the adsorption of TA onto SMZ with CPB patchy bilayer coverage at solution pH 5.5 include the electrostatic attraction, hydrogen bonding, hydrophobic interaction and organic partitioning.

4. Conclusion

Natural zeolite had little affinity for TA in aqueous solution. SMZ presented higher TA adsorption efficiency than natural zeolite, and SMZ with higher loading amount of CPB exhibited higher TA adsorption efficiency. The adsorption kinetics of TA onto SMZ with CPB bilayer coverage was found to follow a pseudo-second-order model. The equilibrium adsorption data of TA onto SMZ with CPB bilayer coverage fitted well with Lamguir, Redlich-Peterson and Sips isotherm models. The calculated thermodynamic parameters showed that the adsorption of TA onto SMZ with CPB bilayer coverage was feasible, spontaneous and exothermic in nature. The TA adsorption capacity for SMZ with CPB bilayer coverage slightly decreased with increasing ionic strength but significantly increased with increasing Cu(II) concentration. For SMZ with CPB bilayer coverage, TA adsorption capacity was relatively high at solution pH 4.0–7.0, and decreased with increasing solution pH from 7.0 to 8.5. For SMZ with monolayer coverage, TA adsorption capacity was slightly influenced by solution pH at 4.0–7.0. The main mechanism controlling TA onto SMZ with CPB monolayer coverage is hydrophobic interaction. The mechanisms controlling TA adsorption onto SMZ with CPB bilayer coverage at solution pH 5.5 include electrostatic attraction, hydrogen bonding and organic partitioning.

References

[1] J.H. Wang, S.R. Zheng, J.L. Liu, Z.Y. Xu, Tannic acid adsorption on amino-functionalized magnetic mesoporous silica , Chem. Eng. J. 165 (2010) 10–16.
[2] J.N. Wang, A.M. Li, L. Xu, Y. Zhou, Adsorption of tannic and gallic acids on a new polymeric adsorbent and the effect of Cu(II) on their removal , J. Hazard. Mater. 169 (2009) 794–800.
[3] J.H. Wang, C.L. Zheng, S.L. Ding, H.R. Ma, Y.F. Ji, Behaviors and mechanisms of tannic acid adsorption on an amino-functionalized magnetic nanoadsorbent , Desalination 273 (2011) 285–291.
[4] P.C. Chiang, E.E. Chang, P.C. Chang, C.P. Huang, Effects of pre-ozonation on the removal of THM precursors by coagulation , Sci. Total Environ. 407 (2009) 5735–5742.
[5] W.W. Li, X.D. Li, K.M. Zeng, Aerobic biodegradation kinetics of tannic acid in activated sludge system , Biochem. Eng. J. 43 (2009) 142–148.
[6] Y. Sun, A.M. Li, Q.X. Zhang, J.L. Chen, D.F. Fu, S.H. Wang, Adsorptive separation of tannic acid from aqueous solution by polymeric resins , Sep. Sci. Technol. 43 (2008) 389–402.
[7] T.S. Anirudhan, M. Ramachandran, Adsorptive removal of tannin from aqueous solutions by cationic surfactant-modified bentonite clay , J. Colloid Interface Sci. 299 (2006) 116–124.
[8] J.H. Huang, Y.F. Liu, X.G. Wang, Selective adsorption of tannin from flavonoids by organically modified attapulgite clay , J. Hazard. Mater. 160 (2008) 382–387.
[9] J.H. An, S. Dultz, Adsorption of tannic acid on chitosan-montmorillonite as a function of pH and surface charge properties , Appl. Clay Sci. 36 (2007) 256–264.
[10] T.S. Anirudhan, P.S. Suchithra, Adsorptive characteristics of tannin removal from aqueous solutions and coir industry effluents using calcined and uncalcined hydrotalcites , Ind. Eng. Chem. Res. 46 (2007) 4606–4613.
[11] Ç. Sarıcı-Özdemir, Y. Önal, Equilibrium, kinetic and thermodynamic adsorptions of the environmental pollutant tannic acid onto activated carbon , Desalination 251 (2010) 146–152.
[12] F. Liu, X.G. Luo, X.Y. Lin, Adsorption of tannin from aqueous solution by deacetylated konjac glucomannan , J. Hazard. Mater. 178 (2010) 844–850.
[13] S.B. Wang, Y.L. Peng, Natural zeolites as effective adsorbents in water and wastewater treatment , Chem. Eng. J. 156 (2010) 11–24.
[14] Y. Zeng, H. Woo, G. Lee, J. Park, Adsorption of Cr(VI) on hexadecylpyridinium bromide (HDPB) modified natural zeolites , Microporous Mesoporous Mater. 130 (2010) 83–91.
[15] R. Leyva-Ramos, A. Jacobo-Azuara, P.E. Diaz-Flores, R.M. Guerrero-Coronado, J. Mendoza-Barron, M.S. Berber-Mendoza, Adsorption of chromium(VI) from an aqueous solution on a surfactant-modified zeolite , Colloid Surf. A 330 (2008) 35–41.
[16] Z. Li, H.L. Hong, Retardation of chromate through packed columns of surfactant-modified zeolite , J. Hazard. Mater. 162 (2009) 1487–1493.
[17] Z. Li, R.S. Bowman, Counterion effects on the sorption of cationic surfactant and chromate on natural clinoptilolite , Environ. Sci. Technol. 31 (1997) 2407–2412.
[18] P. Chutia, S. Kato, T. Kojima, S. Satokawa, Adsorption of As(V) on surfactant-modified natural zeolites , J. Hazard. Mater. 162 (2009) 204–211.
[19] J. Hrenovic, M. Rozic, L. Sekovanic, A. Anic-Vucinic, Interaction of surfactant-modified zeolites and phosphate accumulating bacteria , J. Hazard. Mater. 156 (2008) 576–582.
[20] H. Guan, E. Bestland, C.Y. Zhu, H.L. Zhu, D. Albertsdottir, J. Hutson, C.T. Simmons, M. Ginic-Markovic, X. Tao, A.V. Ellis, Variation in performance of surfactant loading and resulting nitrate removal among four selected natural zeolites , J. Hazard. Mater. 183 (2010) 616–621.
[21] J. Schick, P. Caullet, J. Paillaud, J. Patarin, C. Mangold-Callarec, Nitrate sorption from water on a surfactant-modified zeolite. Fixed-bed column experiments , Microporous Mesoporous Mater. 142 (2011) 549–556.
[22] J. Schick, P. Caullet, J. Paillaud, J. Patarin, C. Mangold-Callarec, Batch-wise nitrate removal from water on a surfactant-modified zeolite , Microporous Mesoporous Mater. 132 (2010) 395–400.
[23] M. Rožić, Đ. Ivanec Šipušić, L. Sekovanić, S. Miljanić, L. Ćurković, J. Hrenović, Sorption phenomena of modification of clinoptilolite tuffs by surfactant cations , J. Colloid Interface Sci. 331 (2009) 295–301.
[24] A. Kuleyin, Removal of phenol and 4-chlorophenol by surfactant-modified natural zeolite , J. Hazard. Mater. 144 (2007) 307–315.
[25] J.A. Simpson, R.S. Bowman, Nonequilibrium sorption and transport of volatile petroleum hydrocarbons in surfactant-modified zeolite , J. Contam. Hydrol. 108 (2009) 1–11.
[26] X.Y. Jin, M.Q. Jiang, X.Q. Shan, Z.G. Pei, Z.L. Chen, Adsorption of methylene blue and orange II onto unmodified and surfactant-modified zeolite , J. Colloid Interface Sci. 328 (2008) 243–247.
[27] Y. Dong, D.Y. Wu, X.C. Chen, Y. Lin, Adsorption of bisphenol A from water by surfactant-modified zeolite , J. Colloid Interface Sci. 348 (2010) 585–590.
[28] S.G. Wang, W.X. Gong, X.W. Liu, B.Y. Gao, Q.Y. Yue, Removal of fulvic acids using the surfactant modified zeolite in a fixed-bed reactor , Sep. Purif. Technol. 51 (2006) 367–373.
[29] Y.H. Zhan, J.W. Lin, Y.L. Qiu, N.Y. Gao, Z.L. Zhu, Adsorption of humic acid from aqueous solution on bilayer hexadecyl trimethyl ammonium bromide modified zeolite , Front. Environ. Sci. Eng. China 5 (2011) 65–75.
[30] S.R. Taffarel, J. Rubio, Adsorption of sodium dodecyl benzene sulfonate from aqueous solution using a modified natural zeolite with CTAB , Miner. Eng. 23 (2010) 771–779.
[31] Y.H. Zhan, J.W. Lin, Z.L. Zhu, Removal of nitrate from aqueous solution using cetylpyridinium bromide (CPB) modified zeolite as adsorbent , J. Hazard. Mater. 186 (2011) 1972–1978.
[32] M.A. Wahab, S. Jellali, N. Jedidi, Ammonium biosorption onto sawdust: FTIR analysis, kinetics and adsorption isotherms modeling , Bioresour. Technol. 101 (2010) 5070–5075.
[33] E. Ramos-Ramírez, N.L. Gutiérrez Ortega, C.A. Contreras Soto, M.T. Olguín Gutiérrez, Adsorption isotherm studies of chromium (VI) from aqueous solutions using sol-gel hydrotalcite-like compounds , J. Hazard. Mater. 172 (2009) 1527–1531.
[34] C.B. Vidal, A.L. Barros, C.P. Moura, A.C.A. de Lima, F.S. Dias, L.C.G. Vasconcellos, P.B.A. Fechine, R.F. Nascimento, Adsorption of polycyclic aromatic hydrocarbons from aqueous solutions by Modified Periodic Mesoporous Organosilica , J. Colloid Interface Sci. 357 (2011) 466–473.

[35] Q.S. Liu, T. Zheng, P. Wang, J.P. Jiang, N. Li, Adsorption isotherm, kinetic and mechanism studies of some substituted phenols on activated carbon fibers , Chem. Eng. J. 157 (2010) 348–356.

[36] T.S. Anirudhan, P. Senan, Adsorption characteristics of cytochrome C onto cationic Langmuir monolayers of sulfonated poly(glycidylmethacrylate)-grafted cellulose: mass transfer analysis, isotherm modeling and thermodynamics , Chem. Eng. J. 168 (2011) 678–690.

[37] Z.H. Wang, B. Xiang, R.M. Cheng, Y.J. Li, Behaviors and mechanism of acid dyes sorption onto diethylenetriamine-modified native and enzymatic hydrolysis starch , J. Hazard. Mater. 183 (2010) 224–232.

[38] Z. Li, R. Beachner, Z. McManama, H. Hanlie, Sorption of arsenic by surfactant-modified zeolite and kaolinite , Microporous Mesoporous Mater. 105 (2007) 291–297.

[39] C.L. Ding, C. Shang, Mechanisms controlling adsorption of natural organic matter on surfactant-modified iron oxide-coated sand , Water Res. 44 (2010) 3651–3658.

[40] Y. Park, G.A. Ayoko, R.L. Frost, Characterisation of organoclays and adsorption of p-nitrophenol: environmental application , J. Colloid Interface Sci. (2011), doi:10.1016/j.jcis.2011.04.085.

[41] B. Sarkar, Y.F. Xi, M. Megharaj, G.S.R. Krishnamurti, D. Rajarathnam, R. Naidu, Remediation of hexavalent chromium through adsorption by bentonite based Arquad® 2HT-75 organoclays , J. Hazard. Mater. 183 (2010) 87–97.

[42] C.W. Oo, M.J. Kassim, A. Pizzi, Characterization and performance of Rhizophora apiculata mangrove polyflavonoid tannins in the adsorption of copper (II) and lead (II) , Ind. Crop Prod. 30 (2009) 152–161.

[43] M. Özacar, İ.A. Şengil, H. Türkmenler, Equilibrium and kinetic data, and adsorption mechanism for adsorption of lead onto valonia tannin resin , Chem. Eng. J. 143 (2008) 32–42.

[44] Y.F. Xi, M. Mallavarapu, R. Naidu, Adsorption of the herbicide 2 4-D on organo-palygorskite , Appl. Clay Sci. 49 (2010) 255–261.

[45] M. Majdan, E. Sabah, M. Bujacka, S. Pikus, A. Płaska, Spectral and equilibrium properties of phenol-HDTMA- and phenol-BDMHDA-bentonite as a response to the molecular arrangements of surfactant cations , J. Mol. Struct. 938 (2009) 29–34.

[46] M.A. Nawi, S. Sabar, A.H. Jawad, Sheilatina, W.S. Wan Ngah, Adsorption of Reactive Red 4 by immobilized chitosan on glass plates: towards the design of immobilized TiO$_2$-chitosan synergistic photocatalyst-adsorption bilayer system , Biochem. Eng. J. 49 (2010) 317–325.